Global Energy Interconnection
Development and Cooperation Organization

ELSEVIER
Production And Hosting By Elsevier On Behalf Of KeAi
KeAi

Volume 3 Number 4 August 2020 (324-334)
DOI: 10.14171/j.2096-5117.gei.2020.04.003

Global Energy Interconnection

Contents lists available at ScienceDirect
https: //www.sciencedirect.com/journal/global-energy-interconnection

Full-length article

Small-current grounding fault location method based on transient main resonance frequency analysis

Yongjie Zhang[1], Xiaojun Wang[1], Junjuan Li[2], Yin Xu[1], Guohong Wu[3]

1. School of Electrical Engineering, Beijing Jiaotong University, Beijing, 100044, China
2. State Grid Lanzhou Electric Power Company, Lanzhou, Gansu, 730070, China
3. Dept. Of Electrical & Electronics Eng., Tohoku Gakuin University, 1-13-1, Chuo, Tagajo, Miyagi Prefecture, 9858537, Japan

Scan for more details

Abstract: The small-current grounding fault in distribution network is hard to be located because of its weak fault features. To accurately locate the faults, the transient process is analyzed in this paper. Through the study we take that the main resonant frequency and its corresponding component is related to the fault distance. Based on this, a fault location method based on double-end wavelet energy ratio at the scale corresponding to the main resonant frequency is proposed. And back propagation neural network (BPNN) is selected to fit the non-linear relationship between the wavelet energy ratio and fault distance. The performance of this proposed method has been verified in different scenarios of a simulation model in PSCAD/EMTDC.

Keywords: Small-current grounding fault location, Main resonant frequency, Double-end wavelet energy ratio, Back-propagation neural network (BPNN).

1 Introduction

Single-phase-to-ground faults in arc suppression coil grounding distribution networks are typical weak-feature faults. When the fault occurs, the fault current is only several amperes because of the compensation of the arc-suppression coil. The small-current grounding faults has small steady-state zero-sequence current and indistinguishable features. Accurate small-current grounding fault location methods are still a serious problem.

Compared with the transmission network, the distribution network has the characteristics of complex network structure, short lines, and numerous branches. In addition, traditional fault location methods are limited in line-cable hybrid lines and multi-branch lines.

At present, the research on fault location of transmission grids is relatively mature, and the fault location of small-current grounding distribution networks is mostly extended by the transmission grid location methods. According to the adopted data, existing location methods can be divided into two categories: steady-state-data-based methods and transient-data-based methods.

The impedance-based method is one of the most typical steady-state-data-based methods [1-6]. Its main principle is to determine the fault location by assuming that the

Received: 8 May 2020/ Accepted: 28 June 2020/ Published: 25 August 2020

✉ Xiaojun Wang
xjwang1@bjtu.edu.cn

Yongjie Zhang
18117032@bjtu.edu.cn

Junjuan Li
1427158231@qq.com

Yin Xu
xuyin@bjtu.edu.cn

Guohong Wu
wugh@mail.tohoku-gakuin.ac.jp

parameters of transmission line are uniform and the circuit impedance of fault line is proportional to the distance length of fault line. But the performance of impedance-based method is greatly affected by the line parameters, fault resistance, and pre-fault power flow [7, 8]. Another type of steady-state-data-based methods is voltage-distribution based method. According to the different principles, it can be divided into two types. The first principle is that the fault point has the lowest voltage of the whole line. Through finding the point of lowest voltage, the fault can be located [9, 10]. Another principle is the voltages calculated from both sides are the same. So the fault location can be determined by calculating the voltage from both ends of line [11-13].

For the transient-data-based fault location methods, the traveling-wave-based methods are the most typical type. The traveling-wave-based methods achieve fault location by adopting the features of traveling wave refraction with combining the wave velocity and transmission time. Specifically, it can be divided into single-end traveling-wave-based methods and double-end traveling-wave-based methods [14-15]. Reference [16] proposed a double-end traveling-wave-based method to locate the fault by selecting the first three differences according to the sequence of time of traveling wave head reaching the line end. To solve the problem of different wave velocities of hybrid lines, a normalization algorithm of wave velocities is proposed [17]. Some methods achieve fault location based on the relationship by combining the characteristic frequencies of fault transient traveling waves, wave velocities, and the location of fault points [18-20]. The traveling-wave-based methods have accurate location results when the measurements are accurate. But its application is limited by the short length of lines in distribution networks and expensive cost.

The medium and low frequency transient information of small current grounded distribution system is abundant. The transient magnitude can reach several times of the steady state magnitude, and the transient is not affected by arc suppression coil compensation, which contains abundant fault information. Another type of transient-data-based fault location method is based on transient feature extraction of corresponding frequency. The relationship between frequency of transient feature and fault distances is firstly proposed in [21]. According to the fault waveform, a self-adaptive modified mother wavelet function is established to improve the accuracy of fault location method [22]. In these years, the development of distribution-level phasor measurement units (D-PMUs) brings high sampling time-stamped waveform data, which makes transient synchronized information available in distribution networks [23]. Some D-PMU-based fault location methods have been proposed [24]. For the better application of features, machine learning algorithms have also been adopted in recent researches [25-27].

In this paper, we proposed a novel transient-data-based fault location method. Through the main resonance frequency analysis, the frequency bands including the most transient information are determined with considering relative influences. Then, the double-end wavelet transient energy ratio under the corresponding frequency bands is selected as the feature. To fit the non-linear relationship between the extracted features and fault distances, a back propagation neural network (BPNN) is introduced here. Meanwhile, the application of the proposed method in hybrid lines and multi-branch lines is considered and analyzed. The performances are verified by a 4-feeder arc suppression coil grounding distribution network is simulated in PSCAD/EMTDC.

2 Transient main resonance frequency analysis

In this section, we analyze the transient main resonance frequency and its influences. For an RLC series circuit, as shown in Fig. 1, the frequency of the sinusoidal voltage source U_S is variable. R, L, C are corresponding to resistance, inductance, and capacitance, respectively. The equivalent impedance of the port in the above loop can be expressed as follows:

$$Z(j\omega) = R + j(\omega L - \frac{1}{\omega C}) = R + jX \tag{1}$$

where ω is the angular frequency, and X is the equivalent reactance. Because the frequency effects of the inductor and capacitor are opposite, there must be a frequency ω_0 at which $X = 0$ in the above equation. The inductive reactance value in the loop is equal to the capacitive reactance value. In other words, the inductance is equal to the capacitance in this circuit. At this moment, the entire circuit exhibits a purely resistive state, which is defined as the resonance state of the circuit.

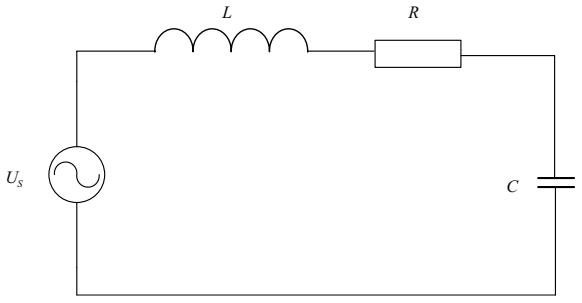

Fig. 1 RLC series circuit

The equivalent circuit of transient analysis after single-phase small-current grounding fault is shown in Fig. 2. R=2(R_{s1}+R_{L1})+R_{L0}+3R_k, where R_{s1} and R_{L1} represent the line-mode loop resistances, R_{L0} is the zero-mode loop resistance, and R_k is the fault resistance. L=2(L_{s1}+L_{L1})+L_{L0} represents the sum of the line circuit inductance and the zero-mode loop inductance. Where, L_{s1} and R_{s1} are the inductance and resistance of the source. L_{L1} and R_{L1} are the inductance and resistance of line between fault point to the source. L_p represents the inductance of the arc suppression coil.

Fig. 2 Equivalent circuit for the single-phase ground fault transient analysis of a low-current grounded system

When the fault ground resistance is relatively low, and the influence of the arc suppression coil is not considered, the transient process is composed of the energy conversion between L and C. During this period, several resonance states are established, and the transient current can be expressed as follows.

$$i = I_{Cm}\left(\frac{\omega_f}{\omega} sin\varphi sin\omega_f t - cos\varphi cos\omega_f t\right)e^{-\delta t} \quad (2)$$

where I_{Cm} is the amplitude of capacitance current and φ is the angle of fault current and supply voltage. δ is the decay factor, which is equal to R/2L. ω_f is the free oscillation angular frequency of the transient current, which represents a series of frequency values corresponding to the transient current harmonic values. Among the many frequencies, there is a resonance frequency with the highest current energy in the low-frequency band, namely the main resonance frequency. Its calculation formula is as shown in (3).

$$\omega_f = \sqrt{\frac{1}{LC_0} - (\frac{R}{2L})^2} \quad (3)$$

For a metallic fault, ω_f can be simplified as follows.

$$\omega_f \approx \sqrt{\frac{1}{LC_0}} = \sqrt{\frac{1}{\left(L_{u0}l_f + 2L_{u1}l_f + 2L_{T1}\right)C_{0\Sigma}}} \quad (4)$$

where L_{u0}, L_{u1}, and L_{T1} are the pre-unit line zero-mode inductance, metallic-mode inductance, and transformer's metallic-mode inductance, respectively. l_f is the distance between the fault and the bus line, and $C_{0\Sigma}$ is the ground capacitance of all the lines.

From the above equation, we find that the main resonant frequency is related to the resistance, capacitance, and inductance of the equivalent loop. In the equivalent loop, the inductance is related to the fault distance, the capacitance is related to the fault distance and the system-to-ground capacitance, and the resistance and fault distance are transition resistance is related. Therefore, the main resonant frequency is determined by the fault distance, the system-to-ground capacitance, and the transition resistance. The farther the fault distance, the lower the main resonance frequency. When the transition resistance is relatively low, the influence can be neglected. When the transition resistance is high enough, the main resonance frequency will decrease accordingly.

The amplitude corresponding to the main resonant frequency component can be expressed as follows:

$$A = \frac{1}{\sqrt{2}} I_{Cm}\sqrt{[(\frac{\omega_f}{\omega}\sin\varphi)^2 + (\cos\varphi)^2} \quad (5)$$

Clearly, the main resonant frequency component is affected by the fault distance, system-to-ground capacitance, transition resistance, and fault initial phase angle.

3 Double-end wavelet energy ratio

3.1 Wavelet transform and wavelet transient energy spectrum

Wavelet transform is an effective transient information extraction algorithm that can effectively solve the problem of non-stationary signal analysis. At different resolutions, the details of a signal can help characterize different physical structures. The low-resolution details can be used to characterize large structures, and with the increase in the resolution, finer details can be obtained. Through the wavelet transform, the feature information in the full frequency domain can be obtained [28-30]. However, a continuous wavelet transform requires a large amount of computation and is unsuitable for practical applications. Although discrete wavelet transform effectively solves this problem, spectral aliasing is observed between the components, which limits the accuracy of the signal analysis.

In 1988, Mallat combined existing research and explained the orthogonal wavelet through a mathematical function analysis. A multi-resolution analysis was proposed for the first time. The multi-resolution analysis is based on the function space concept, and the signal is in different levels of space. The basic idea behind decomposition, i.e., showing a signal with different resolutions, is the use of functions of different scales to continuously approximate the original signal, so this method is also called the multi-scale analysis [31]. Moreover, Mallat proposed a general

construction method for orthogonal wavelets and a fast algorithm for orthogonal wavelet transform, namely the Mallat decomposition algorithm. The Mallat decomposition algorithm, also known as the tower algorithm, involves decomposing a signal through a high-pass filter and low-pass filter layer-by-layer to obtain a series of high-frequency and low-frequency components. This process is equivalent to dividing time-domain signals into frequency bands in the frequency domain. The specific formulae are as follows.

$$A_0[f(t)] = f(t) \tag{6}$$

$$A_j[f(t)] = \sum_k A_{j-1} H(2n-k)[f(t)] \tag{7}$$

$$D_j[f(t)] = \sum_k A_{j-1} G(2n-k)[f(t)] \tag{8}$$

where $f(t)$ is the original signal, j is the number of decomposition layers, and H and G are the wavelet low-pass filter decomposition coefficient and high-pass filter decomposition coefficient in the time-frequency. A_j is the approximation coefficient, which represents the corresponding low-frequency components, and D_j is the detail coefficient corresponding to the high-frequency components. The signal is subdivided layer-by-layer to obtain the characteristic information of the signal in the different frequency bands.

The energy of a signal is expressed as the sum of the squares of the amplitudes of the signals at each point. According to the law of conservation of energy, the energy of a signal in the time domain is equal to its energy in the frequency domain. Therefore, the frequency-domain energy after wavelet transform can also fully represent the signal characteristics. Let the wavelet transform coefficient of the jth layer of the original signal be W_j(k). Then, the wavelet energy of the signal at this scale is defined as the integral of the square of W_j(k) along the time axis:

$$E_j = \sum_{k=1}^{N} \left| W_j(k) \right|^2 \tag{9}$$

where N is the sampling window width of the signal. The wavelet energy spectrum of the discrete signal is $E = [E_1, E_2, \cdots E_j \cdots]$. After wavelet decomposition, the wavelet energy of j different frequency bands can be obtained. The wavelet energy values of the different frequency bands indicate that the signal is proportional to the total energy in the frequency band.

3.2 Analysis of double-end wavelet energy ratio

The main resonance frequency and its components are affected not only by the fault distance, but also by the fault resistance and fault initial phase angle. Under different fault resistances and fault initial phase angles, the difference in the wavelet energy is relatively large. To avoid the influence of fault resistance and fault initial phase angle on the wavelet energy, the ratio of the two-terminal energy of the fault line is used as the characteristic quantity.

Fig. 3 shows the variation in the energy ratio of a single-end wavelet to a double-end wavelet with the fault distance at a certain scale under different transition resistances. Figs. 3(a) and (b) show that the zero-mode voltage wavelet energy at the head and at the end of the line varies with the fault distance and fault resistance, respectively. The single-end voltage wavelet energy varies with the fault distance. Moreover, the wavelet energy increases at a higher rate with the decrease in the fault resistance. Fig. 3(c) shows the variations in the energy ratio of the wavelets at the head and at the end of the line with the fault distance and resistance. After the two-terminal ratio calculation, the wavelet energy ratio varies with the fault distance; however, it varies only

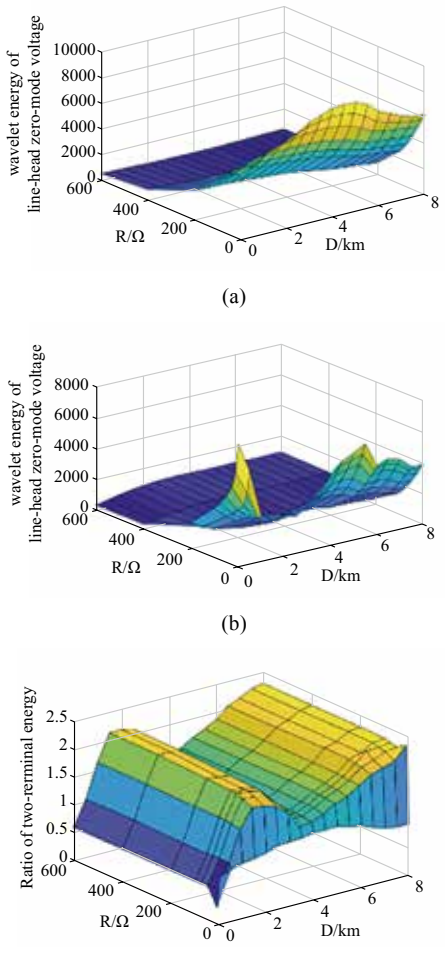

Fig. 3 Variations in the ratio of single-end wavelet energy to double-end wavelet energy with the fault distance under different fault resistances

slightly under different fault resistances. Therefore, the ratio of the two-terminal wavelet energy can help eliminate the influence of fault resistance on the wavelet energy.

Similarly, we obtain the variations in the ratio of single-end wavelet energy to double-end wavelet energy of the line at different initial fault angles, as shown in Fig. 4.

In summary, when a fault occurs at different locations in a low-current grounded system, the influences of fault resistance and fault initial phase angle can be eliminated by the energy ratio of the two-terminal wavelet. Therefore, we selected the double-end wavelet energy ratio at a scale corresponding to the main resonance frequency as the fault feature. Moreover, we adopt the neural network to fit the nonlinear relationship between the wavelet energy ratio and the fault distance. Thus, the low-current grounded faults can be located.

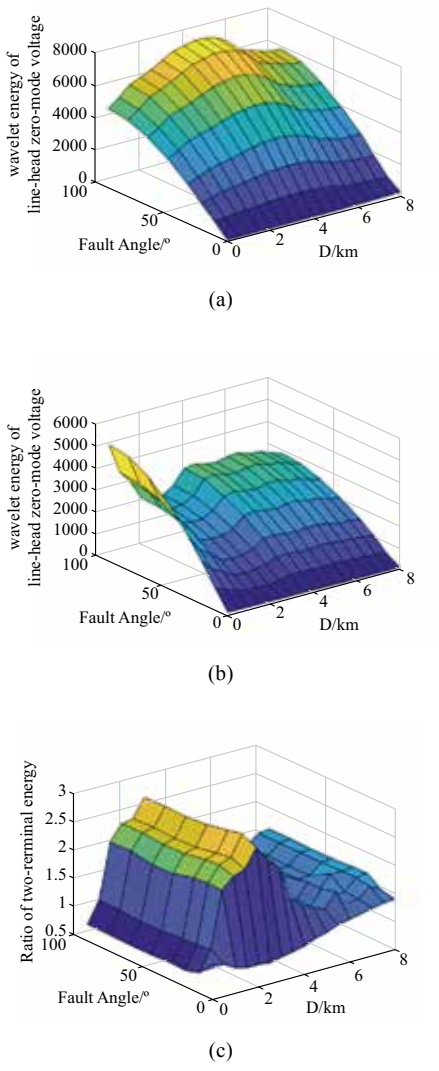

Fig. 4 Variation in the ratio of single-end wavelet energy to double-end wavelet energy under different fault angles

4 Low-current grounding fault location method

4.1 Instruction and parameter settings

To fit the nonlinear relationship between the wavelet energy ratio and the fault distance, the BPNN is selected in this study. The basic idea of the BPNN is to learn certain rules through the training of its own network when there is no definite mathematical mapping equation relationship between the input and output, and obtain the result closest to the expected output value at a specific input value. The basic algorithm is the gradient descent method, which uses the gradient search technique to minimize the mean square error of the actual output value and the expected output value of the network [32].

There are two main factors when training the BPNN: the quality of the extracted features and the setting of the training scenarios. In this study, the extracted features are double-end wavelet energy ratios. To extract the key transient features, the wavelet parameters should be carefully considered.

In this study, "db3" is selected as the mother wavelet based on the experimental test. The number of layers of the wavelet decomposition can be determined from the equation below.

$$N=\min[round(\log 2(f/1000)+1), round(\log 2(f/100)-1)] \quad (10)$$

where f is the sampling rate of the waveform. The sampling rate of the waveform data provided by D-PMUs can reach 10 kHz. Therefore, the wavelet decomposition layer is set as 5 under this sampling rate. Fig. 5 shows a schematic of the corresponding frequency bands at each scale obtained by the decomposition of the five-layer wavelet transform. Evidently, after the five-layer decomposition, the range of the main resonance frequency is included, and the fault information in the main resonance frequency band is extracted.

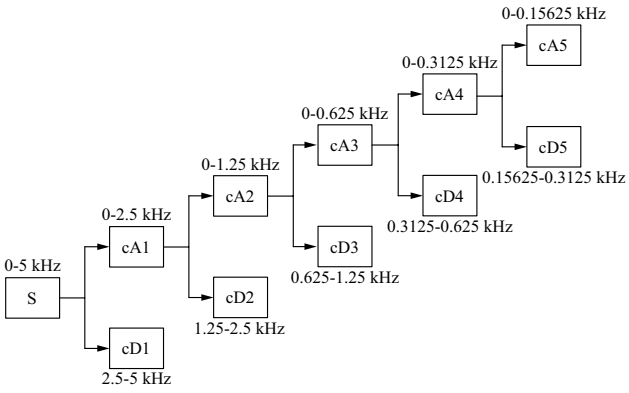

Fig. 5 Schematic of five-layer wavelet transform decomposition

To analyze the effect of the time window, the spectrum diagrams corresponding to zero-mode currents in the 1 cycle, 3/4 cycle, 1/2 cycle, and 1/4 cycle are obtained, as shown in Fig. 6. The setting of the time window can only influence the amplitude, not the transient main resonant frequency. In this study, to ensure that the transient information is included, we selected 1 cycle as the time window.

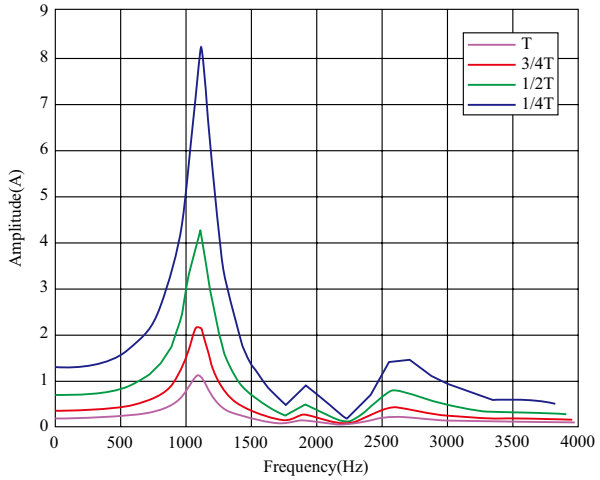

Fig. 6 Zero-sequence current spectrum under different time windows

To determine the chosen layers for fault location, the spectral range corresponding to the transient zero-mode current of the entire line should be calculated. Subsequently, the energy ratios under the decomposition layers that cover the spectral range are selected as features.

With an overhead line as an example, Fig. 7 shows the transient zero-sequence current spectrum diagram corresponding to different fault locations in the entire line. The main resonance frequency range is between 500 Hz and 1500 Hz, corresponding to the cD2 and cD3 decomposition layers.

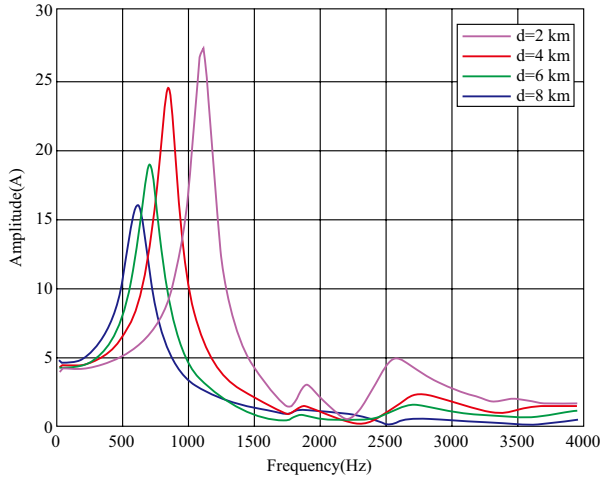

Fig. 7 Zero-sequence current spectrum of overhead line faults

To verify the effect of the number of layers, the location errors when using different decomposition layers are compared, as shown in Fig. 8. As illustrated, the more the number of layers selected, the better the positioning effect. However, an excessive number of layers does not make the fault positioning effect any better. This is because the transient main resonant frequency includes most of the temporary information in the state component, which can represent the basic characteristics of the transient process. When the number of layers is too low, the fault information cannot be fully represented, and the positioning error is very high. When the two-layer wavelet energy ratio is selected as the input sample, the location error is within 500 m. Therefore, the cD2 and cD3 two-layer wavelet energy ratio is selected as the input sample for the neural network.

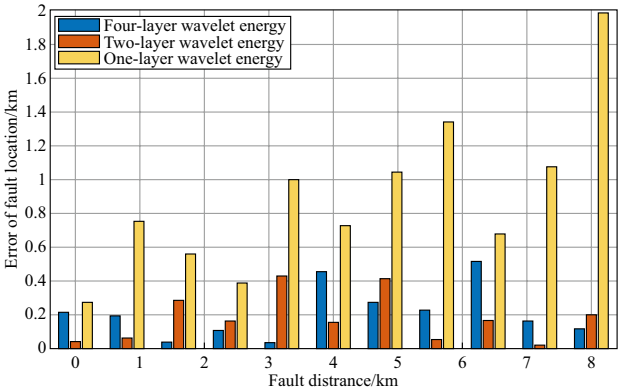

Fig. 8 Location error when using different layers of wavelet energy ratio

4.2 Application of complex line structures

A distribution network contains many hybrid lines (combination of overhead lines and cables) and multi-branch lines. In this section, the applicability of the proposed method is analyzed.

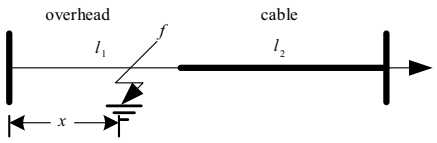

Fig. 9 Hybrid line fault

Fig. 9 shows the fault diagram of the overhead-cable hybrid line. The lengths of the overhead lines and cables are l_1 and l_2, respectively, and the fault distance is x. After fault occurrence, the spectrum of the zero-sequence current overlaps because of the two different parameters of the overhead line and cable, and the spectrum of the zero-mode current contains two frequencies with high amplitudes. By combining the two frequencies, we can obtain the

comprehensive frequency band, and calculate the wavelet energy ratio at the corresponding scales. At this time, the nonlinear relationship between the double-end wavelet energy ratio and the fault distance is a segmentation function.

$$F(x)=\begin{Bmatrix} F_1(x) & x\leqslant l_1 \\ F_2(x) & l_1<x\leqslant l_2 \end{Bmatrix} \tag{11}$$

In the above equation, the piecewise function F is continuous at the overhead line-cable mixing point $x = l_1$. Therefore, if the training samples are sufficient, the neural network can be used to fit the piecewise function. In other words, the proposed method can also be applied to the hybrid lines.

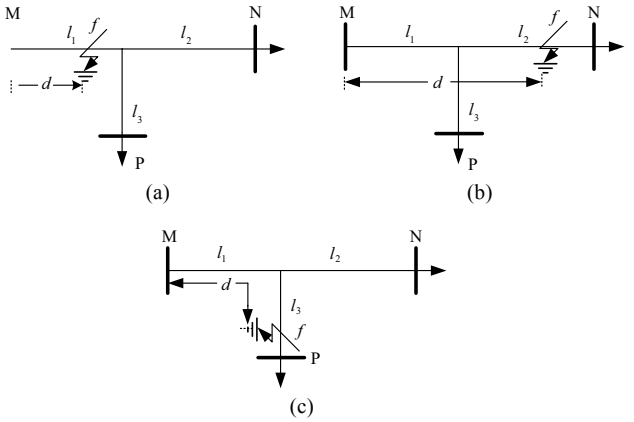

Fig. 10 Multi-branch line fault

Fig. 10 shows a schematic of a fault occurring in a distribution network with branch lines. The lengths of the three lines are l_1, l_2, and l_3, and the fault may occur at any point on the three lines. The measuring device is installed at three points M, N, and P, and the wavelet energy ratio of MN, NP, and PM is constructed as the location criterion of the line. The corresponding functional relationships are set as $F1$, $F2$, and $F3$ respectively. The corresponding neural networks are trained, and the fault distances x_1, x_2, and x_3 are located using the three networks, respectively. x_1, x_2, and x_3 represent the distances from the fault location to the corresponding ends. Based on the relationship between x_1, x_2, x_3 and l_1, l_2, l_3, the fault branch and the positioning result can be determined.

For the l_1 line fault, the network associated with the branch is $F1$ and $F3$. The fault distance obtained by the $F1$ should be less than the length of the l_1 branch. The fault distance obtained by $F3$ minus the length of the l_3 branch should be less than the length of the l_1 branch and greater than zero. In other words, the network $F1$ and $F3$ positioning results satisfy the relationship:

$$\begin{Bmatrix} x_1<l_1 \\ 0<x_3-l_3<l_1 \end{Bmatrix} \tag{12}$$

When determining whether a fault occurs on line l_1, the location distance from the M terminal is taken as the average value of the location results of $F1$ and $F2$ on line l_1.

$$d=\frac{x_1+l_1-(x_3-l_3)}{2} \tag{13}$$

Similarly, any low-current grounded faults occurring at the other lines can also be located. Table 1 presents the location result determination table.

Table 1 Location result decision table

Fault line	l_1	l_2	l_3
Branch decision	$\begin{cases} x_1<l_1 \\ 0<x_3-l_3<l_1 \end{cases}$	$\begin{cases} x_2<l_2 \\ 0<x_1-l_1<l_2 \end{cases}$	$\begin{cases} x_3<l_3 \\ 0<x_2-l_2<l_3 \end{cases}$
Location average x	$\frac{x_1+l_1-(x_3-l_3)}{2}$	$\frac{x_2+l_2-(x_1-l_1)}{2}$	$\frac{x_3+l_3-(x_3-l_2)}{2}$
Distance from M-terminal	$d=x$	$d=l_1+(l_2-x)$	$d=l_1+(l_3-x)$

5 Simulation and verification

To verify the proposed method, a 10 kV four-feeder arc suppression coil grounded distribution network is simulated in PSCAD/EMTDC, as shown in Fig. 11. $L1$ is an 8 km overhead line, $L2$ is a 6 km cable line, and $L3$ is a hybrid line with a 5 km overhead line and a 3 km cable line. $L4$ is a 15 km overhead multi-branch line, where l_1, l_2, and l_3 are 6, 5, and 4 km, respectively. The parameters of the lines are shown below. For the overhead lines, the positive-sequence impedance is Z=0.034+j0.286 Ω/km, and the positive-sequence admittance is Y=j0.406×10^{-5} S/km. The zero-sequence impedance is Z=0.286+j1.421 Ω/km, and the zero-sequence admittance is Y=j0.155×10^{-5} S/km. For the cable line, the impedance matrix and admittance matrix are shown below.

$$Z=\begin{bmatrix} 0.2+j2.019 & 0.002+j0.0004 & -0.002+j0.0004 \\ -0.002+j0.0004 & 0.052+j0.089 & -0.004+j0.0007 \\ 0.002+j0.0004 & -0.004+j0.0007 & 0.052+j0.089 \end{bmatrix} \ \Omega/\text{km}$$

$$Y=\begin{bmatrix} j0.198 & 0 & 0 \\ 0 & j0.198 & 0 \\ 0 & 0 & j0.198 \end{bmatrix}\times 10^{-3} \ \text{S/km}$$

The setting of the training scenarios for the BPNN is shown below.

(1) Fault resistance: 0.01, 10, 25, 50, 75, 100, 200, 400, and 600 Ω.

(2) Fault angle: 0, 10, 20, 30, 45, 60, 75, and 90°.

(3) Fault distance: Starting from the beginning of the line, we set a fault point every 0.5 km.

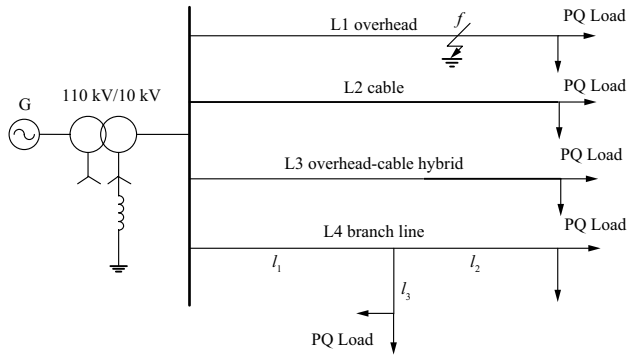

Fig. 11 Simulation topology of a low-current grounded system

5.1 Fault location results for the overhead line

Fig. 12 shows the verification result of the fault locations in the overhead line. The location results are represented by "+," and the errors are shown in the corresponding bar chart. The location errors of the proposed method in the different positions of the overhead line are within 500 m.

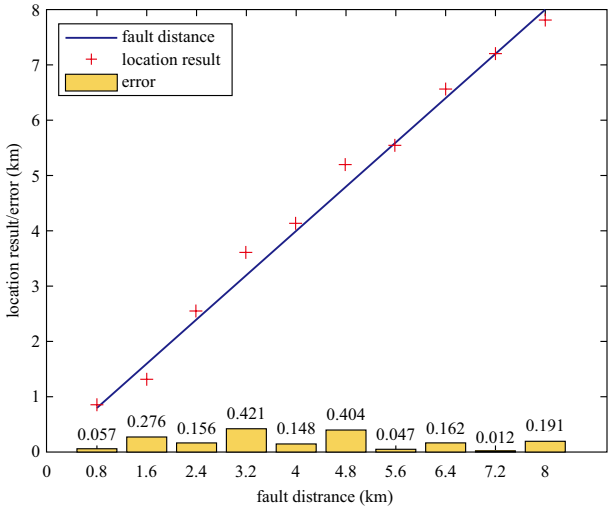

Fig. 12 Location results of over-head line under different fault distances

To verify the effect of fault resistances, we set the fault distance 3 km away from the bus, and the fault initial angle is set to 90°. The fault resistances are set as 0, 20, 40, 60, 80, 150, 300, and 500 Ω. Fig. 13 shows the verification results. The errors under the different fault resistances are all within 500 m. The proposed method is less affected by the fault resistances.

Subsequently, the location results under different fault initial angles are verified. The fault initial angles are set to 0, 5, 10, 15, 50, 70, and 90°. The fault location is 6.2 km, and the fault resistance is 10 Ω. Fig. 14 shows the location results. Clearly, when the initial phase angle of the fault is

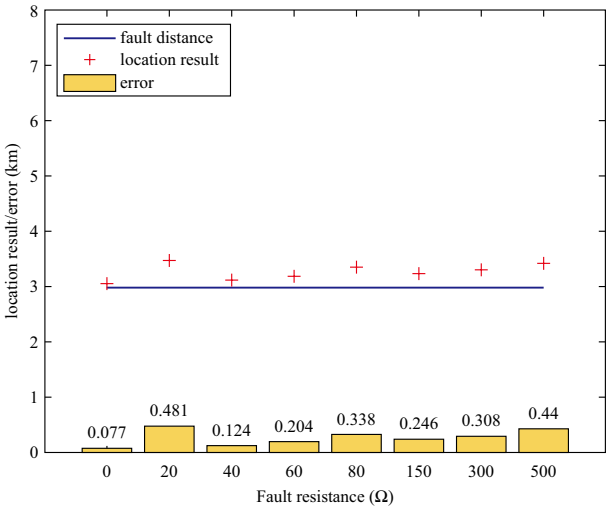

Fig. 13 Location results of over-head line under different fault resistances

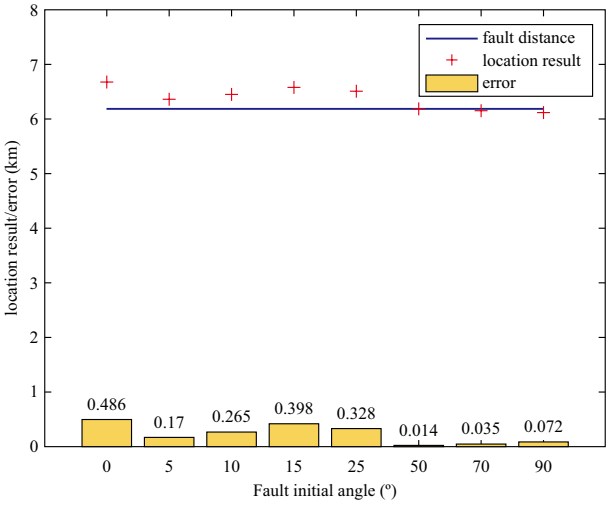

Fig. 14 Location results of over-head line under different fault angles

small, the location error is relatively greater than the large fault initial angle. The errors remain within 500 m. Thus, the proposed method can accurately locate faults without getting affected by the fault initial angle.

5.2 Fault location results for the cable line

Similarly, we verified the proposed method for the faults in the cable line. Fig. 15 shows the fault location results. As shown, the location errors are within 300 m, thus demonstrating the performance of the proposed method for cable lines.

5.3 Fault location results for the hybrid line

Fig. 16 shows the fault location results for the hybrid line. The location errors are all within 300 m, and the proposed method has good performance at positions near the hybrid points.

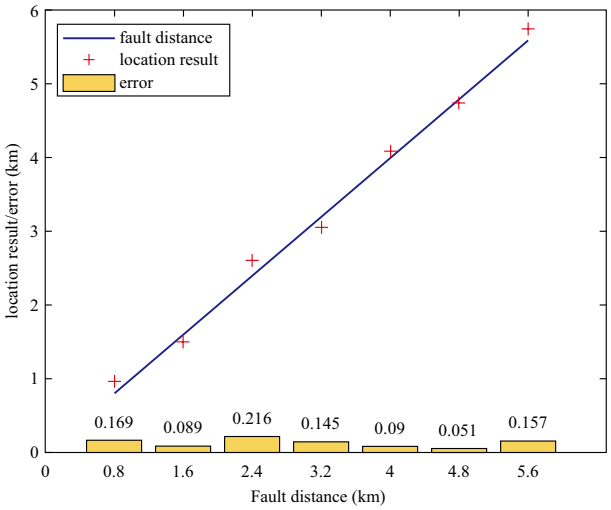

Fig. 15 Location results of cable line under different fault distances

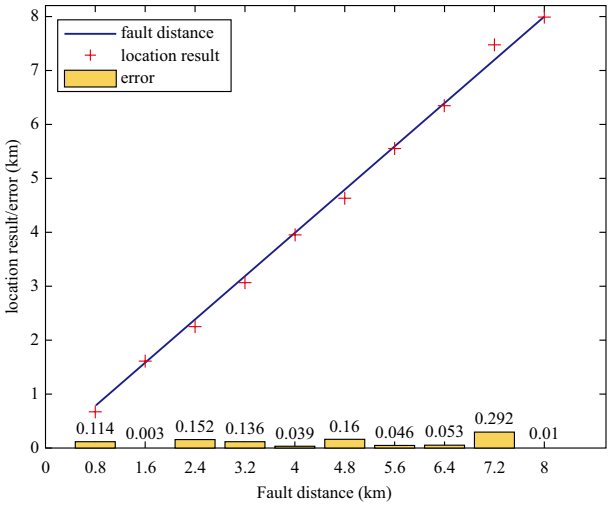

Fig. 16 Location results of hybrid line under different fault distances

5.4 Fault location results for a multi-branch line

Finally, the location results for the multi-branch line are verified, as listed in Table 2. The error in the location results under the different positions is less than 600 m. In conclusion, based on the method introduced in Section 4.2, the proposed method can accurately determine the branch line and locate the faults.

Table 2 Location results when faults occur in different positions with branch lines

Fault branch and distance from the fault point to the M end /km	Branch result	Location result /km	Location error /km
L1, 0.3	L1	0.089	0.211
L1, 1.5	L1	1.673	0.173
L1, 4.5	L1	4.904	0.404
L1, 5.7	L1	5.307	0.393
branch point, 6.0	L2	5.841	0.103
L2, 6.3	L2	6.390	0.090
L2, 7.5	L2	8.027	0.527
L2, 10.7	L2	10.397	0.303
L3, 6.2	L3	6.202	0.002
L3, 8.5	L3	8.021	0.479
L3, 9.7	L3	9.100	0.600

6 Conclusion

In this study, we developed a low-current grounded fault location method. The analysis of the transient main resonance frequency showed a correlation between the transient main resonance frequency and the fault distance. With this information, the faults in the system could be located accurately through the double-end wavelet energy ratio corresponding to the main resonance frequency and the BPNN. The verification results showed that the proposed method is less affected by the fault distances, fault resistances, fault initial angle, and line structures.

The proposed method can locate the fault accurately, but it needs sufficient historical data, which may restrict its application. In practice, a practical alternative is to establish an online training mechanism. The initial training data of the fitting model are obtained from simulation or laboratory platforms. Then, during the operation of the distribution network, the training samples are continuously revised through data of actual cases. Another feasible method is training the fitting model by integrating data of multi distribution networks. But this method needs to consider the feature scales and communication. Further research will focus on solving this problem. The proposed method will be relatively complex when the line has a number of branches. The fast branch determination method is worth more attention.

Acknowledgements

This work was supported by National Key R&D Program of China (2017YFB0902800) and Science and

Technology Project of State Grid Corporation of China (52094017003D).

References

[1] Krishnathevar R, Ngu EE (2012) Generalized impedance-based fault location for distribution systems. IEEE Trans Power Deliv 27(1):449-451

[2] Salim RH, Salim KCO, Bretas AS (2011) Further improvements on impedance-based fault location for power distribution systems, IET Gener Transm Distrib 5(4):467-478

[3] Gong Y, Guzmán A (2013) Integrated fault location system for power distribution feeders. IEEE Trans Ind Appl 49(3):1071-1078

[4] Dasthti R, Sadeh J (2014) Fault section estimation in power distribution network using impedance-based fault distance calculation and frequency spectrum analysis. IET Gener Transm Distrib 8(8):1406-1417

[5] Lotfifard S, Kezunovic M, Mousavi MJ (2011) Voltage sag data utilization for distribution fault location. IEEE Trans Power Deliv 26(2): 1239-1246

[6] Xia Jingde, Zhang Xiangcong, Huang Xinbo, et al. (2015) New algorithm of fault location based on longitudinal impedance for two-terminal quantities. Power Automation Equipment, 35(10):133-139

[7] García-Gracia M, El Halabi N, Martín Arroyo SM et al. (2011) Application of a distance relaying scheme to compensate fault location errors due to fault resistance. Electr Power Syst Res 81(8):1681-1687

[8] García-Gracia M, El Halabi N, Borroy S et al. (2011) Phase jump correction factor applied to the differential equation algorithm by an adaptive scheme. IET Gener Transm Distrib 5(2):266-275

[9] Zhang Y, Li B, Jiang X, Li Z (2015) A fault location method for extra-high voltage mixed line based on variation of sequence voltage. 2015 5th International Conference on Electric Utility Deregulation and Restructuring and Power Technologies (DRPT), Changsha, 2015:916-921

[10] Liu R, Tai N, Fan C, Huang W, Liu Z (2018) Research on accurate fault location for multi-terminal transmission lines based on positive sequence components. Power Syst Technol 42(9):3033-3040

[11] Wang X et al. (2019) Distribution network fault location based on PMU information. Power Syst Technol 43(3):810-817

[12] Mu K, Wang F, Liu Y (2017) Asynchronous two-terminal fault location method for unbalanced fault based on parameter identification. High Voltage Eng 43(11):3763-3768

[13] Wang F, Mu K, Zhang J, Liu Y, Qian Y (2018) Asynchronous two-terminal fault location method of transmission line based on parameter modification. Electric Power Automation Equipment, 38(8):95-101

[14] Akmaz D, Mamiş MS, Arkan M, Tağluk ME (2018) Transmission line fault location using traveling wave frequencies and extreme learning machine. Electric Power Syst Res 155:1-7

[15] Gilany M, Ibrahim DK (2006) Traveling-wave-based fault-location scheme for multiend-aged underground cable system. IEEE Trans Power Deliv 22(1):82-89

[16] Jia Huibin, Zhao Haifeng, Fang Qianghua, et al. (2012) Single-phase ground fault location method for distribution network based on multi-terminal traveling wave. Power System Automation, 36 (02):96-100

[17] Yu Cheng, Tang Shengxue (2015) Traveling wave location method for single-phase-to-ground fault of hybrid transmission line based on normalization of wavelet-wave velocity. Electrical appliances and Energy Efficiency Management Technology, 2015(23):11-17

[18] Mamiş MS, Arkan M, Keleş C (2013) Transmission lines fault location using transient signal spectrum. Int J Electrical Power Energy Syst 53:714-718

[19] Wu LY, He ZY, Qian QQ (2008) A single ended fault location method using traveling wave natural frequency. Proceedings of the Chinese Society of Electrical Engineering (CSEE), 28(10):69-75

[20] Borghetti A, Corsi S, Nucci CA et al. (2006) On the use of continuous-wavelet transform for fault location in distribution power systems. Int J Electrical Power Energy Syst 28(9):608-617

[21] Yu Cheng, Tang Shengxue (2015) Traveling wave location method for single-phase-to-ground fault of hybrid transmission line based on normalization of wavelet-wave velocity. Electrical Appliances and Energy Efficiency Management Technology, 2015(23):11-17

[22] Rui L, Zheng J, Jianhua L (2013) A new single-ended traveling wave location method based on fault characteristic frequency. Power Syst Protection Control 41(15):7-13

[23] von Meier A, Stewart E, McEachern A, Andersen M, Mehrmanesh L (2017) Precision micro-synchrophasors for distribution systems: A summary of applications. IEEE Trans Smart Grid 8(6):2926-2936

[24] Ren J, Venkata SS, Sortomme E (2014) An accurate synchrophasor based fault location method for emerging distribution systems. IEEE Trans Power Deliv 29(1):297-298

[25] Zayandehroodi H, Mohamed A, Farhoodnea M, Mohammadjafari M (2013) An optimal radial basis function neural network for fault location in a distribution network with high penetration of DG units. Measurement 46(9):3319-3327

[26] Pourahmadi-Nakhli M, Safavi AA (2011) Path characteristic frequency-based fault locating in radial distribution systems using wavelets and neural networks. IEEE Trans Power Deliv 26(2):772-781

[27] Liang J, Jing T, Niu H, Wang J (2020) Two-terminal fault location method of distribution network based on adaptive convolution neural network. IEEE Access, 8:54035-54043

[28] Mallat SG (1989) Multifrequency channel decompositions of images and wavelet models. IEEE Trans Acoustics Speech & Signal Process 37(12):2091-2102

[29] Borghetti A, Corsi S, Nucci CA (2006) On the use of continuous-wavelet transform for fault location in distribution power systems. Int J Electrical Power Energy Syst 28(9):608-617

[30] Yang Shuying, Wang Lihong, Du Ronghua, et al. (2008)

Selection and application of wavelet bases in power system transient protection. Journal Power System and Automation 20(05):107-110

[31] Mallat S (1996) Wavelets for a vision. Proceedings of the IEEE, 84(4):604-614

[32] Heermann PD, Khazenie N (1992) Classification of multispectral remote sensing data using a back propagation neural network. IEEE Trans Geosci Remote Sens. 30:81-88

Biographies

Yongjie Zhang received the B.Sc. and M.Sc. degrees in electrical engineering from Bejing Jiaotong University, Beijing, China, in 2016 and 2018, respectively. He is currently pursuing the Ph.D. degree with Beijing Jiaotong University. His research interests include weak fault detection and application of machine learning in distribution network.

Xiaojun Wang received the B.Sc., M.Sc., and Ph.D. degrees in electrical engineering from North China Electric Power University, Beijing, China, in 2001, 2004, and 2008, respectively. From 2014 to 2015, he went abroad in ALSTOM GRID Ltd. (England) with BOND project. He is currently an Associate Professor with Beijing Jiaotong Uni-versity, Beijing. His main research interests are integrated energy system and application of artificial intelligence in electrical engineering.

Junjuan Li received the B.Sc. and M.Sc. degrees in electrical engineering from Bejing Jiaotong University, Beijing, China, in 2017 and 2019, respectively. She is currently working at the State Grid Lanzhou Electric Power Company. Her main research direction is power system relay protection.

Yin Xu received the B.E. and Ph.D. degrees in electrical engineering from Tsinghua University, Beijing, China, in 2008 and 2013, respectively. From 2013 to 2016, he was an Assistant Research Professor with the School of Electrical Engineering and Computer Science, Washington State University, Pullman, WA, USA. He is currently a Professor with Beijing Jiaotong Univ-ersity, Beijing, China. His research interests include power system resilience, urban electricity-transportation integrated system, and power system high-performance simulation.

Dr. Xu is currently serving as Chair of Energy Internet Resilience Working Group under IEEE PES Energy Internet Coordinating Committee and Secretary of the Distribution Test Feeder Working Group under the IEEE PES Distribution System Analysis Subcommittee.

Guohong Wu received his B.S. and M.S. degrees in electrical engineering from Tianjin University, China in 1989 and 1994, respectively. In 1998, he received a joint-supervised Ph.D. degree from the University of Tokyo, Japan and Tianjin University, China. He was with the University of Tokyo and Tohoku University, Japan from 1995 to 2005. He is currently a professor with Department of Electrical Engineering and Information Technology at Tohoku Gakuin University, Japan. His research interests include renewable energy generation technologies, power system stability analysis, FACTS devices, superconductivity application to power systems, HVDC systems, etc. He is a member of IEEE and IEE-Japan.

(Editor Zhou Zhou)